Available online at www.sciencedirect.com
SCIENCE DIRECT®
Journal of Sound and Vibration 267 (2003) 933–954
JOURNAL OF SOUND AND VIBRATION
www.elsevier.com/locate/jsvi

Vibration and stability of cracked hollow-sectional beams

D.Y. Zheng[1], S.C. Fan*

School of Civil and Environmental Engineering, Nanyang Technological University, Nanyang Avenue, Singapore 639798, Singapore

Received 12 March 2002; accepted 10 December 2002

Abstract

This paper presents simple tools for the vibration and stability analysis of cracked hollow-sectional beams. It comprises two parts. In the first, the influences of sectional cracks are expressed in terms of flexibility induced. Each crack is assigned with a local flexibility coefficient, which is derived by virtue of theories of fracture mechanics. The flexibility coefficient is a function of the depth of a crack. The general formulae are derived and expressed in integral form. It is then transformed to explicit form through 128-point Gauss quadrature. According to the depth of the crack, the formulae are derived under two scenarios. The first is for shallow cracks, of which the penetration depth is contained within the top solid-sectional region. The second is for deeper penetration, in which the crack goes into the middle hollow-sectional region. The explicit formulae are best-fitted equations generated by the least-squares method. The best-fitted curves are presented. From the curves, the flexibility coefficients can be read out easily, while the explicit expressions facilitate easy implementation in computer analysis. In the second part, the flexibility coefficients are employed in the vibration and stability analysis of hollow-sectional beams. The cracked beam is treated as an assembly of sub-segments linked up by rotational springs. Division of segments are made coincident with the location of cracks or any abrupt change of sectional property. The crack's flexibility coefficient then serves as that of the rotational spring. Application of the Hamilton's principle leads to the governing equations, which are subsequently solved through employment of a simple technique. It is a kind of modified Fourier series, which is able to represent any order of continuity of the vibration/buckling modes. Illustrative numerical examples are included.

1. Introduction

The dynamic behaviour of a cracked beam is of significant importance in engineering. It attracts the attention of many researchers. Dimarogonas [1] presented the state-of-art review of

*Corresponding author. Tel.: +65-67905299; fax: +65-67910676.
E-mail addresses: dingyang.zheng@jcu.edu.au (D.Y. Zheng), cfansc@ntu.edu.sg (S.C. Fan).
[1] Presently, a post-doctoral research fellow at James Cook University, Australia.

0022-460X/03/$ - see front matter © 2003 Elsevier Ltd. All rights reserved.
doi:10.1016/S0022-460X(02)01605-X

various methods in tackling a cracked structural member. Till now, many publications have reported on this subject. Amongst the many easily accessible ones some notable ones are Refs. [2–23], etc. They all dealt with cracked beams/plates having solid rectangular or circular cross-sections. However, in many practical applications, in particular in bridge engineering, structural members have other forms of cross-sections such as rectangular/trapezoidal hollow sections or multi-cellular hollow sections. Against this background, this paper focuses on the vibration analyses of beams having hollow cross-sections.

Firstly, by virtue of the theory of fracture mechanics, general integral formulae are derived for the equivalent flexibility coefficients of a local crack. The integral form is hard to use. For practical purpose, it is then transformed to explicit form through employment of 128-point Gauss quadrature. The explicit formulae are best-fitted equations generated by the least-squares method. The best-fitted curves are also presented. From the curves, the flexibility coefficients can be read out easily, while the explicit expressions facilitate easy implementation in computer analysis.

The flexibility coefficients are then employed in the vibration and stability analysis of hollow-sectional beams. The cracked beam is firstly divided into sub-segments, which are linked up by hinges and rotational springs. Division of segments are made coincident with the location of cracks or any abrupt change of sectional property. The crack's flexibility coefficient then serves as that of the rotational spring. In this paper, it is assumed that the cracks are always open and the beam is in the range of linear elasticity. Applying Hamilton's principle to the model leads to the governing equations, which are subsequently solved through employment of a simple technique [20,21]. It is a kind of modified Fourier series, which is able to represent a function with internal geometrical discontinuity, and hence it emerges to be a convenient tool to represent the vibration/buckling modes having any order of continuity. Subsequently, illustrative numerical examples are given.

2. Local flexibility due to a crack in solid rectangular-sectional beam

Let a denote the penetration depth of a sectional crack (Fig. 1) in a rectangular section of depth h and width b, M be a virtual twin couple (moment) applied across the crack location and θ be the relative rotation of that cracked section, we have [24]

$$\theta = \frac{\partial}{\partial M}\left[\int_{A_c} G\,\mathrm{d}A\right] = \frac{\partial}{\partial M}\left[\int_0^a \int_{-b/2}^{b/2} G\,\mathrm{d}\eta\,\mathrm{d}\xi\right], \tag{1}$$

where ξ and η are location variables. ξ is measured along the depth direction of the sectional crack, η is the distance offset from the central vertical axis. A_c $(= a\times b)$ is the surface area of the open crack, and G is a measure of the energy-release rate. In general, G is a function of the applied couple M and the location variables ξ $(0\leqslant\xi\leqslant a)$ and η. In this particular case, the sectional crack is a constant through-width crack. Therefore, G is independent of the width variable η, and hence the equation becomes

$$\theta = \frac{\partial}{\partial M}\left[\int_{A_c} G\,\mathrm{d}A\right] = \frac{\partial}{\partial M}\left[\int_0^a bG\,\mathrm{d}\xi\right]. \tag{1a}$$

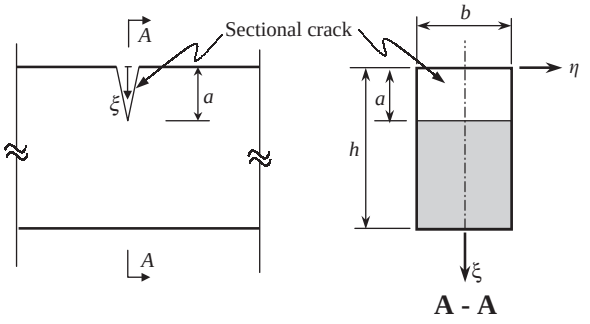

Fig. 1. A sectional crack in a solid rectangular-sectional beam.

The energy-release rate G over a small area ($d\xi \times d\eta$) can be related to the stress intensity factor K_I as follows [3]:

$$G\,d\xi\,d\eta = \frac{K_I^2}{E'}d\xi\,d\eta, \tag{2}$$

where E' is Young's modulus. For plane-stress problem, $E' = E$. For plane-strain problem, $E' = E/(1-\mu^2)$, in which μ is the Poisson ratio.

The presence of the crack induces local flexibility to the beam. The local flexibility coefficient C can be expressed as follows:

$$C = \frac{\partial\theta}{\partial M} = \frac{\partial^2}{\partial M^2}\left[\int_0^a bG\,d\xi\right]. \tag{3}$$

The stress intensity factor K_I in the near region of a crack tip can be expressed as [25]

$$K_I = \frac{Mh}{2I_0}\sqrt{\pi\xi}F, \tag{4}$$

where I_0 ($= bh^3/12$) is the second moment of the sectional area, and $\boldsymbol{F}$ is a function of the relative position x ($= \xi/h$), i.e.,

$$F = \frac{\sqrt{2/\pi x\tan\pi x/2}[0.923 + 0.199(1-\sin\pi x/2)^4]}{\cos\pi x/2}. \tag{5}$$

Substituting Eq. (4) into Eq. (2) and subsequently the result into Eq. (3) leads to

$$C = \frac{72\pi}{E'bh^2}\int_0^{a/h} xF^2\,dx, \tag{6a}$$

In dimensionless form,

$$CE'bh^2 = 72\pi\int_0^{a/h} xF^2\,dx. \tag{6b}$$

Eqs. (6a) and (6b) are the general integral form of the local flexibility induced by a sectional crack. Explicit form can be obtained through employment of Gauss quadrature [26,27]. Firstly, approximate values are obtained by 128-point quadrature. Then, applying the least-squares

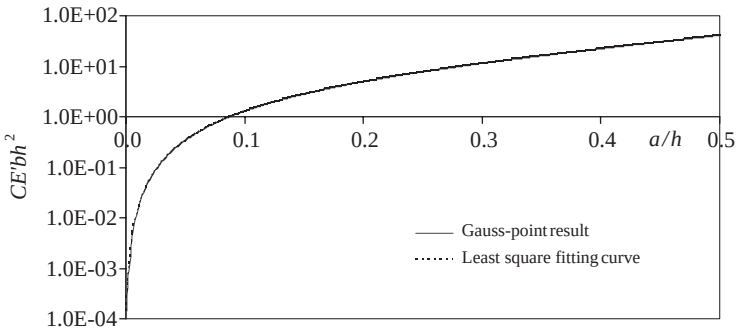

Fig. 2. Dimensionless local flexibility versus relative depth of a crack in a solid rectangular-sectional beam.

method yields the best-fitted explicit expression as given in Eq. (A.1). Both the fitted curve and the Gauss-point values are plotted in Fig. 2. The curve is fitted so nicely that they are hardly distinguishable.

3. Local flexibility due to a sectional crack in solid circular-sectional beam

Let a denote the penetration depth of a sectional crack (see Fig. 3) in a circular section of diameter D (or radius R); M be a virtual twin couple (moment) applied across the crack location and θ be the relative rotation of that cracked section, we have a similar relation as Eq. (1) between θ and the energy-release rate G:

$$\theta = \frac{\partial}{\partial M}\left[\int_{A_c} G \, \mathrm{d}A\right] = \frac{\partial}{\partial M}\left[\int_0^a \int_{-b'}^{b'} G \, \mathrm{d}\eta \, \mathrm{d}\xi\right], \tag{7}$$

where ξ and η denote the same geometrical variables as in Eq. (1), but in this case, the surface area A_c of the open crack is a segment of a round circle and the width of the section is no longer constant. The parameter b' denotes the half-width of a horizontal section measured at a depth ξ. It has a geometric relation with the depth variable ξ, i.e.,

$$b' = \sqrt{R^2 - (R-\xi)^2} = \sqrt{\frac{D^2}{4} - \left(\frac{D}{2} - \xi\right)^2}. \tag{8}$$

Note that in this case, the energy-release rate G is a function of M, the depth variable $\xi(0 \leqslant \xi \leqslant a)$ and the width variable η *as* well. Eq. (2) for the relation between energy-release rate G and stress intensity factor K_I holds. Hence, substituting Eq. (2) into Eq. (7) leads to

$$\theta = \frac{\partial}{\partial M}\left[\int_0^a \int_{-b'}^{b'} \frac{K_I^2}{E'} \, \mathrm{d}\eta \, \mathrm{d}\xi\right]. \tag{9}$$

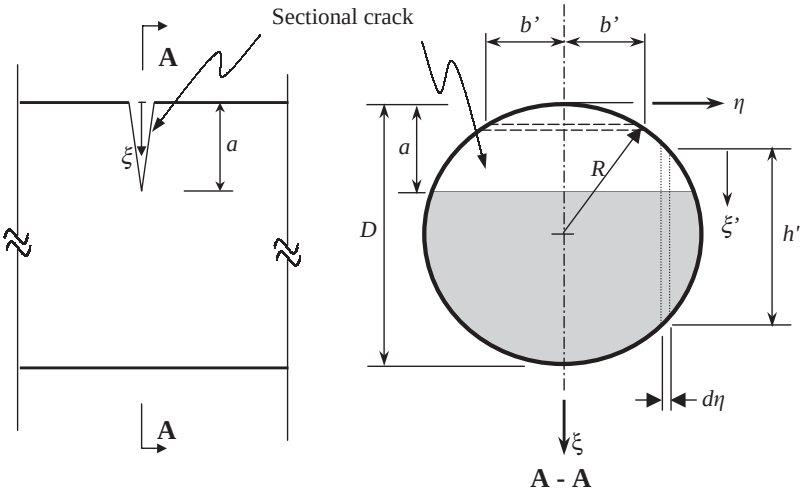

Fig. 3. A sectional crack in a solid circular-sectional beam.

The local flexibility coefficient C can then be expressed as follows:

$$C = \frac{\partial \theta}{\partial M} = \frac{\partial^2}{\partial M^2}\left\{\int_0^a \int_{-b'}^{b'} \frac{K_I^2}{E'}\,\mathrm{d}\eta\,\mathrm{d}\xi\right\}. \tag{10}$$

Consider a small vertical sectional strip, having a small sectional width $\mathrm{d}\eta$ and a depth h', at an arbitrary offset distance η (see Fig. 3). The stress intensity factor has a similar expression as Eq. (4) [25] as follows:

$$K_I = \frac{Mh'}{2I_0}\sqrt{\pi\xi'}F', \tag{11}$$

where I_0 ($= \pi D^4/64$) is the second moment of the whole sectional area, ξ' is a local depth variable measured from the top of that strip, and F' is a function of the local relative position x' ($= \xi'/h'$), i.e.,

$$F' = \frac{\sqrt{2/\pi x' \tan \pi x'/2}[0.923 + 0.199(1 - \sin \pi x'/2)^4]}{\cos \pi x'/2}, \tag{12}$$

in which h' and ξ' have geometric relation with the offset distance η and global depth variable ξ, i.e.,

$$h' = 2\sqrt{R^2 - \eta^2} = 2\sqrt{\frac{D^2}{4} - \eta^2}, \tag{13}$$

$$\xi' = \xi + \sqrt{R^2 - \eta^2} - R = \xi + \sqrt{\frac{D^2}{4} - \eta^2} - \frac{D}{2}. \tag{14}$$

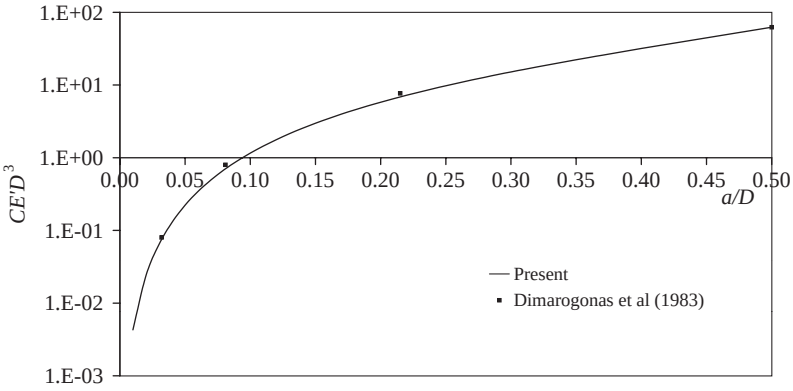

Fig. 4. Dimensionless local flexibility versus relative depth of a crack in a solid circular-sectional beam.

Substituting Eq. (11) into Eq. (10) leads to

$$CE'D^3 = \frac{2048}{\pi}\int_0^a \int_{-b'}^{b'} [1-4(\eta/D)^2](\xi'/D)\boldsymbol{F}'^2(\mathrm{d}\eta/D)(\mathrm{d}\xi/D). \tag{15}$$

Letting $x = \xi/D$ and $y = \eta/D$, we have

$$CE'D^3 = \frac{1024}{\pi}\int_0^{a/D} \left\{ \int_{-\sqrt{x-x^2}}^{\sqrt{x-x^2}} (1-4y^2)(2x+\sqrt{1-4y^2}-1)\boldsymbol{F}'^2\,\mathrm{d}y \right\} \mathrm{d}x, \tag{16}$$

where F' is a function of x' expressed in terms of x and y as follows:

$$x' = \frac{\xi'}{h'} = \frac{2x+\sqrt{1-4y^2}-1}{2\sqrt{1-4y^2}}. \tag{17}$$

Eq. (16) is the general integral form of the local flexibility induced by a sectional crack. Explicit form can be obtained through employment of Gauss quadrature. Firstly, approximate values are obtained by 128×128 quadrature. Then, applying the least-squares method yields the best-fitted explicit expressions as shown in Eqs. (A.2). The best-fitted curve is shown in Fig. 4. Values given by Dimarogonas et al. [3] are also plotted in Fig. 4. Excellent agreement is observed.

4. Local flexibility due to a sectional crack in circular-hollow-sectional beams

4.1. Case 1—shallow open crack $[0 \leqslant a \leqslant (D_e - D_i)/2]$

Fig. 5 shows the shallow open crack, of which the penetration depth 'a' is contained within the top solid-sectional region $[0 \leqslant a \leqslant (D_e - D_i)/2]$. D_e is the external diameter and D_i is the internal diameter. Following the same procedures in deriving the equations for solid circular section, we have a similar expression for the relation between the relative rotation θ and the stress intensity

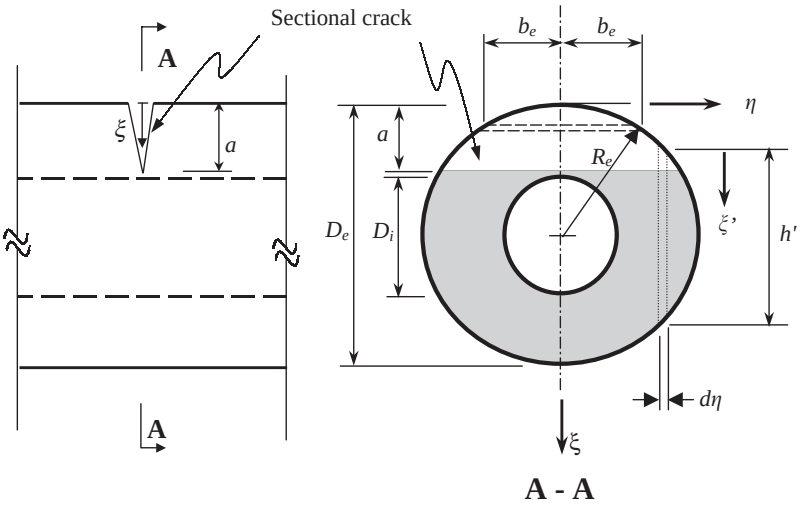

Fig. 5. A sectional crack in a circular-hollow-sectional beam (Case 1).

factor K_I as follows:

$$\theta = \frac{\partial}{\partial M}\left[\int_0^a \int_{-b_e}^{b_e} \frac{K_I^2}{E'}\,\mathrm{d}\eta\,\mathrm{d}\xi\right], \tag{18}$$

where b_e denotes the half-width of a horizontal section measured at a depth ξ. It has a geometric relation with the depth variable ξ, i.e.,

$$b_e = \sqrt{\frac{D_e^2}{4} - \left(\frac{D_e}{2} - \xi\right)^2} \tag{19}$$

and the stress intensity factor K_I has a similar expression as Eq. (11) as follows:

$$K_I = \frac{Mh'}{2\hat{I}_0}\sqrt{\pi\xi'}F', \tag{20}$$

in which $\hat{I}_0\,[= \pi(D_e^4 - D_i^4)/64]$ is the second moment of the whole sectional area.

Substituting Eq. (20) into Eq. (18) and then the result into the definition equation for the local flexibility, i.e., $C = \partial\theta/\partial M$, we can obtain

$$CE'D_e^3 = \frac{2048}{\pi(1-\gamma^4)^2}\int_0^a \int_{-b_e}^{b_e} [1 - 4(\eta/D_e)^2](\xi'/D_e)F'^2(\mathrm{d}\eta/D_e)(\mathrm{d}\xi/D_e), \tag{21}$$

where $\gamma = D_i/D_e$. Letting $x = \xi/D_e$ and $y = \eta/D_e$, we have

$$CE'D_e^3 = \frac{1024}{\pi(1-\gamma^4)^2}\int_0^{a/D_e}\left\{\int_{-\sqrt{x-x^2}}^{\sqrt{x-x^2}}(1-4y^2)(2x+\sqrt{1-4y^2}-1)F'^2\,\mathrm{d}y\right\}\mathrm{d}x, \tag{22}$$

where F' is a function of x' (Eq. (12)), and x' is expressed in terms of x and y exactly as Eq. (17) above.

4.2. Case 2—deeper open crack $[(D_e - D_i)/2 \leqslant a \leqslant (D_e + D_i)/2]$

Fig. 6 shows the deeper open crack, of which the penetration depth 'a' goes into the middle hollow-sectional region $[(D_e - D_i)/2 \leqslant a \leqslant (D_e + D_i)/2]$. Following the same procedures above, we have a similar expression for the relation between the relative rotation θ and the stress intensity factor K_I as follows:

$$\theta = \frac{\partial}{\partial M}\left[\int_0^t \int_{-b_e}^{b_e} \frac{K_I^2}{E'}\,\mathrm{d}\eta\,\mathrm{d}\xi + \int_t^a \int_{-b_e}^{-b_i} \frac{K_I^2}{E'}\,\mathrm{d}\eta\,\mathrm{d}\xi + \int_t^a \int_{b_i}^{b_e} \frac{K_I^2}{E'}\,\mathrm{d}\eta\,\mathrm{d}\xi\right], \tag{23}$$

where $t = (D_e - D_i)/2$, the parameters b_e and b_i denotes, respectively, the external and internal half-width of a horizontal section measured at a depth ξ. They have geometric relations with the depth variable ξ, i.e.,

$$b_e = \sqrt{\frac{D_e^2}{4} - \left(\frac{D_e}{2} - \xi\right)^2}, \quad b_i = \sqrt{\frac{D_i^2}{4} - \left(\frac{D_e}{2} - \xi\right)^2}. \tag{24a, b}$$

Substituting Eq. (20) into Eq. (23) and then the result into the definition equation for the local flexibility, i.e., $C = \partial\theta/\partial M$, we can obtain

$$CE'D_e^3 = \frac{2048}{\pi(1-\gamma^4)^2}\left(\int_0^t \int_{-b_e}^{b_e} + \int_t^a \int_{-b_e}^{-b_i} + \int_t^a \int_{b_i}^{b_e}\right) \times \{[1 - 4(\eta/D_e)^2](\xi'/D_e)F'^2(\mathrm{d}\eta/D_e)(\mathrm{d}\xi/D_e)\}, \tag{25}$$

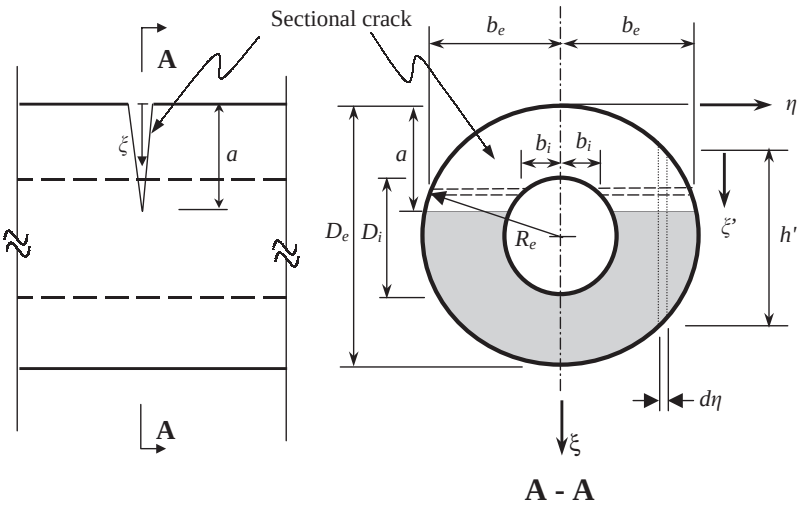

Fig. 6. A sectional crack in a circular-hollow-sectional beam (Case 2).

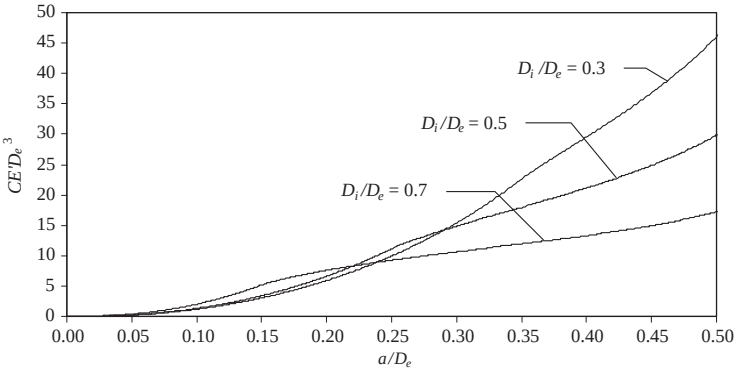

Fig. 7. Dimensionless local flexibility versus relative depth of a crack in a circular-hollow-sectional beam.

where $\gamma = D_i/D_e$. Letting $x = \xi/D_e$ and $y = \eta/D_e$, we have

$$CE'D_e^3 = \frac{1024}{\pi(1-\gamma^4)^2}\left(\int_0^{t/D_e}\int_{-\sqrt{x-x^2}}^{\sqrt{x-x^2}} + \int_{t/D_e}^{a/D_e}\int_{-\sqrt{x-x^2}}^{-\beta} + \int_{t/D_e}^{a/D_e}\int_{\beta}^{\sqrt{x-x^2}}\right) \times \{(1-4y^2)(2x+\sqrt{1-4y^2}-1)F'^2\}\,\mathrm{d}y\,\mathrm{d}x, \tag{26}$$

in which $\beta = \sqrt{x-x^2-(1-\gamma^2)/4}$, and F' is a function of x' (Eq. (12)), and x' is expressed in terms of x and y exactly as Eq. (17) above.

Eqs. (22) and (26) are the general integral form of the local flexibility induced by a sectional crack. Explicit form is obtained firstly through employment of Gauss quadrature and then by the least-squares fitting. The best-fitted explicit expressions for three different diameter ratios ($\tilde{a} =$ 0.3, 0.5 and 0.7) are given in Eqs. (A.3)-(A.5) and the best-fitted curves are shown in Fig. 7.

5. Local flexibility due to a sectional crack in rectangular-hollow-sectional beams

5.1. Case 1—shallow open crack $[0 \leqslant a \leqslant t]$

Fig. 8 shows the shallow open crack, of which the penetration depth 'a' is contained within the top solid-sectional region $[0 \leqslant a \leqslant t]$. '$t$' is the wall thickness, which is constant all around. The hollow section has an overall breadth 'b_0' and height 'h_0'. The internal void's breadth and height are 'b_i' and 'h_i', respectively. Following the same procedures above, we can obtain the dimensionless local flexibility coefficient below:

$$CE'h_0^3 = \frac{72\pi r_b}{[r_b-(r_b-2r_t)(1-2r_t)^3]^2}\int_0^{a/h_0} xF^2\,\mathrm{d}x, \tag{27}$$

where $r_b = b_0/h_0$, $r_t = t/h_0$, and F is a function of x (Eq. (5)).

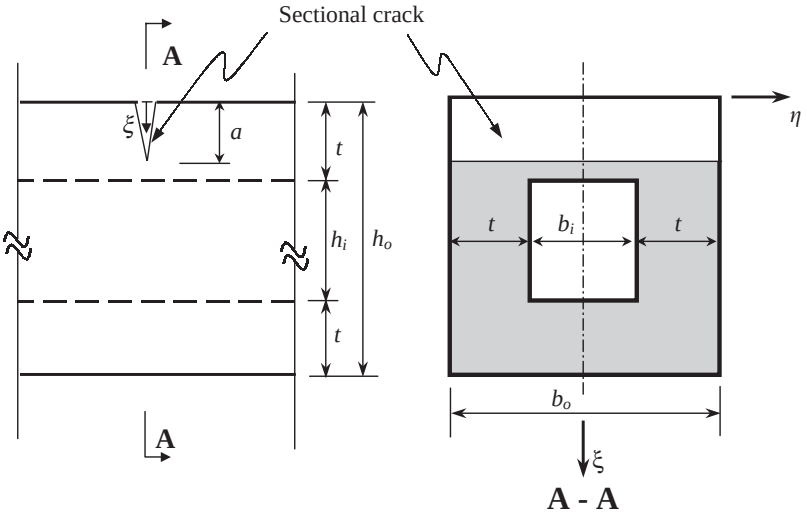

Fig. 8. A sectional crack in a rectangular-hollow-sectional beam (Case 1).

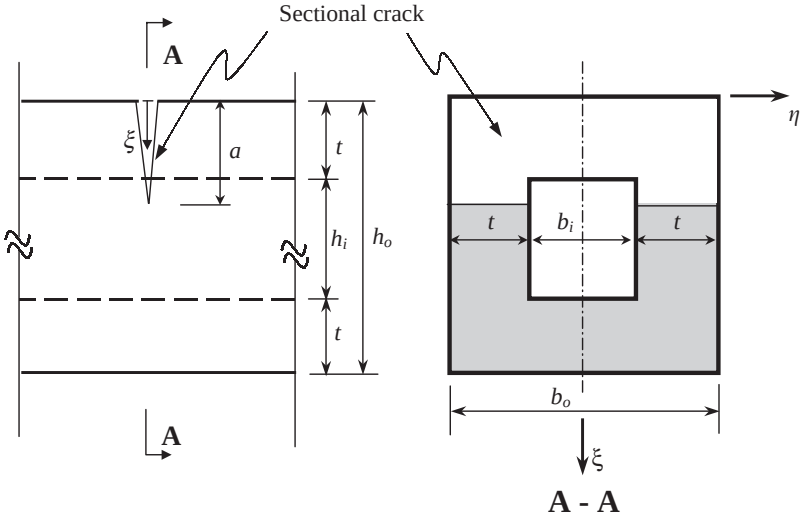

Fig. 9. A sectional crack in a rectangular-hollow-sectional beam (Case 2).

5.2. *Case 2—deeper open crack* $[t \leqslant a \leqslant (h-t)]$

Fig. 9 shows the deeper open crack, of which the penetration depth 'a' goes into the middle hollow-sectional region $[t \leqslant a \leqslant (h-t)]$. Using the same method shown above, we can obtain the dimensionless local flexibility coefficient below:

$$CE'h_0^3 = \frac{72\pi}{[r_b - (r_b - 2r_t)(1-2r_t)^3]^2}\left\{ r_b \int_0^{r_t} xF^2\,\mathrm{d}x + 2r_t \int_{r_t}^{a/h_0} xF^2\,\mathrm{d}x \right\}, \tag{28}$$

where $r_b = b_0/h_0$, $r_t = t/h_0$, and F is a function of x (Eq. (5)).

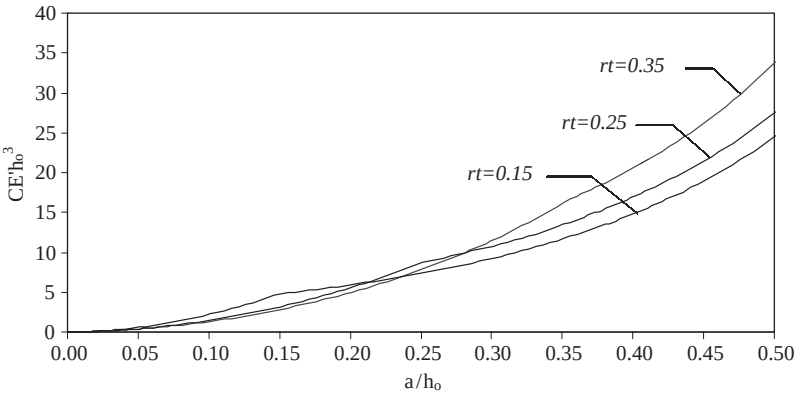

Fig. 10. Dimensionless local flexibility versus relative depth of a crack in a rectangular-hollow-sectional beam ($r_t = t/h_0$).

Eqs. (27) and (28) are the general integral form of the local flexibility induced by a sectional crack. Explicit form is obtained firstly through employment of Gauss quadrature and then by the least-squares fitting. The best-fitted explicit expressions for three different aspect ratios ($r_t = 0.35, 0.25$ and 0.15) of a square hollow section ($r_b = 1.0$) are given in Eqs. (A.6)-(A.8) and the best-fitted curves are shown in Fig. 10.

6. Vibration and stability analysis

A beam having one or more sectional cracks can be modelled as an assembly of sub-beam segments interconnected by virtual springs, which are introduced in to simulate the effects of the open cracks. The vibration/buckling modes of the cracked beam are C^0 continuous at the locations of crack, but higher order continuous at other compact sections. They can be well represented by a kind of C^0 Gibbs phenomenon free Fourier series (GPFFS) functions [28–34].

The deflection of the beam δ at an arbitrary location 'z' and time 't' can be expressed as

$$\delta(z,t) = \sum_{m=1}^{R} q_m(t) Z_m(z) = \mathbf{Z}(z)\mathbf{q}(t), \tag{29}$$

where

$$\mathbf{Z}(z) = \begin{bmatrix} Z_1(z) & Z_2(z) & \cdots & Z_R(z) \end{bmatrix}, \tag{30}$$

$$\mathbf{q}(t) = [\, q_1(t) \quad q_2(t) \quad \cdots \quad q_R(t) \,]^{\mathrm{T}}, \tag{31}$$

in which $Z_m(z)$'s are the assumed vibration/buckling modes of the beam; $q_m(t)$ are the corresponding generalized co-ordinates for the beam.

Combining piece-wise cubic polynomials with the Fourier base function, we can obtain the final form of the representation function, namely GPFFS function

$$Z_m(z) = \bar{Z}_m(z) + \tilde{Z}_m(z). \tag{32}$$

By choosing a proper piece-wise cubic polynomial $\tilde{Z}_m(z)$, we can force the function $Z_m(z)$ to satisfy all the interior discontinuity conditions and any specific boundary conditions. Vibration and stability equations can be obtained through energy formulations [22]:

Vibration equation:

$$(\mathbf{K}_1 + \mathbf{K}_2)\mathbf{q} = \omega^2 \mathbf{M}\mathbf{q}, \tag{33}$$

where

$$\mathbf{K}_1 = \sum_{i=1}^{Q} \int_{z_i}^{z_{i+1}} EI(z)\mathbf{Z}_{,zz}^{\mathrm{T}}(z)\mathbf{Z}_{,zz}(z)\,\mathrm{d}z, \tag{34}$$

$$\mathbf{K}_2 = \sum_{j=2}^{Q} \left[c_{j-1} EI(z_j)\right] \mathbf{Z}_{,zz}^{\mathrm{T}}(z_j)\mathbf{Z}_{,zz}(z_j), \tag{35}$$

$$\mathbf{M} = \int_0^l \rho A(z)\mathbf{Z}^{\mathrm{T}}(z)\mathbf{Z}(z)\,\mathrm{d}z. \tag{36}$$

Stability equation:

$$(\mathbf{K}_1 + \mathbf{K}_2)\mathbf{q} = \lambda \mathbf{K}_G \mathbf{q}, \tag{37}$$

where

$$\mathbf{K}_G = \int_0^l N(z)\mathbf{Z}_{,z}^{T}(z)\mathbf{Z}_{,z}(z)\,\mathrm{d}z. \tag{38}$$

7. Numerical examples

Example 1. *Vibration of a square-hollow-sectional cantilever beam having a crack at the clamped end.*

Fig. 11 shows a square-hollow-sectional cantilever beam having a crack at the clamped end. The geometrical parameters for the beam are: $l = 0.8\,\mathrm{m}$, $b_0 = h_0 = 0.02\,\mathrm{m}$, $r_b = 1.0$, $r_t = 0.25$, $a/h_0 = 0.0 \sim 0.5$. The material parameters are: $E = 210\,\mathrm{GPa}$, $\mu = 0.33$, $\rho = 7800\,\mathrm{kg/m^3}$. The crack is at a fixed location. Cases of various crack depths are studied and results are shown in Fig. 12. The vertical axis in Fig. 12 stands for the natural frequency ratio between the cracked beam and its corresponding intact (un-cracked) beam, i.e., the frequency reduction. The horizontal axis stands for the relative depth of the crack (a/h_0).

Example 2. *Vibration of a circular-hollow-sectional cantilever beam having a crack at the clamped end.*

Fig. 13 shows a hollow circular-hollow-sectional cantilever beam having a crack at the clamped end. The geometrical parameters for the beam are: $l = 0.8\,\mathrm{m}$, $D_e = 0.02\,\mathrm{m}$, $D_i = 0.01\,\mathrm{m}$, $a/D_e = 0.0 \sim 0.5$. The material parameters are: $E = 210\,\mathrm{GPa}$, $\mu = 0.33$, $\rho = 7800\,\mathrm{kg/m^3}$. The crack is at a fixed location. Cases of various crack depths are studied and results are shown in Fig. 14. The

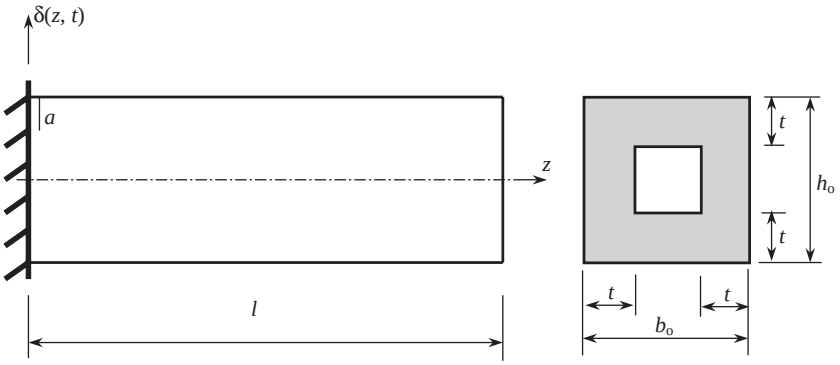

Fig. 11. A square-hollow-sectional cantilever beam having an open crack at the clamped end.

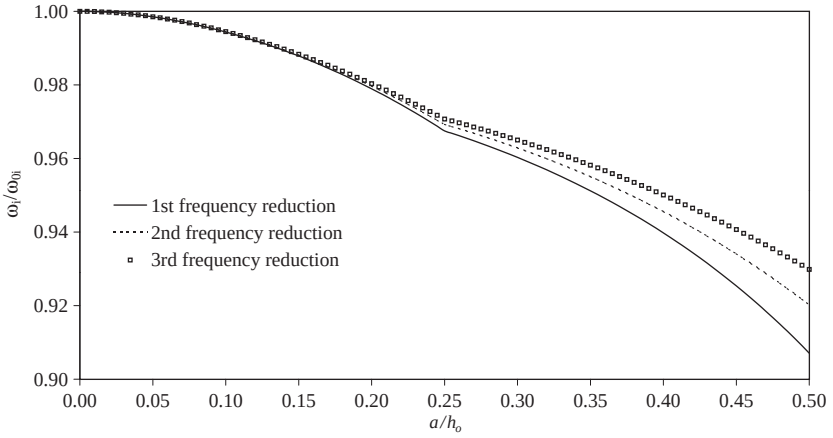

Fig. 12. Frequency reduction of a square-hollow-sectional cantilever beam having an open crack at the clamped end ($r_b = 1.0, r_t = 0.25$).

vertical axis in Fig. 14 stands for the frequency reduction, while the horizontal axis stands for the relative depth of the crack (a/D_e).

Example 3. *Vibration of a circular-hollow-sectional cantilever beam with a crack of varying location.*

The same beam as in Example 2 is considered. The crack has a fixed depth ($a = 0.0075$ m) but its location varies ($z_{c1} = 0.001-0.78$ m). Results are shown in Fig. 15. The vertical axis in Fig. 15 stands for the frequency reduction, while the horizontal axis stands for the location of crack.

Example 4. *Stability of a circular-hollow-sectional cantilever beam having a crack at various locations.*

The same beam as in Example 3 is considered. The crack has a fixed depth ($a = 0.0075$ m) but its location varies ($z_{c1} = 0.001-0.78$ m). Results are shown in Fig. 16. The vertical axis in

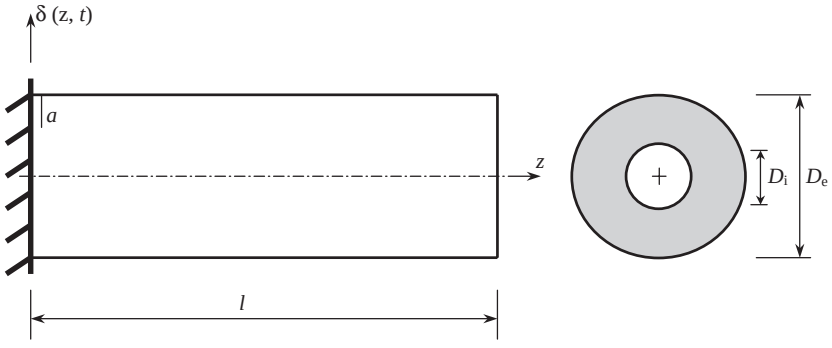

Fig. 13. A circular-hollow-sectional cantilever beam having an open crack at the clamped end.

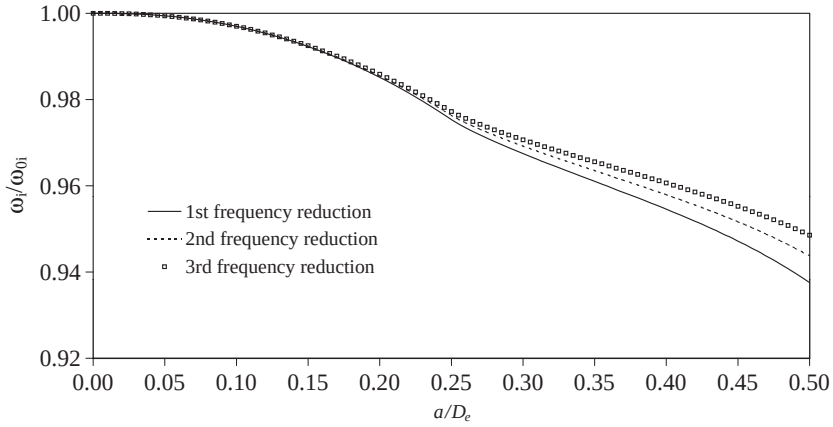

Fig. 14. Frequency reduction of a circular-hollow-sectional cantilever beam having an open crack at the clamped end ($D_i/D_e = 0.5$).

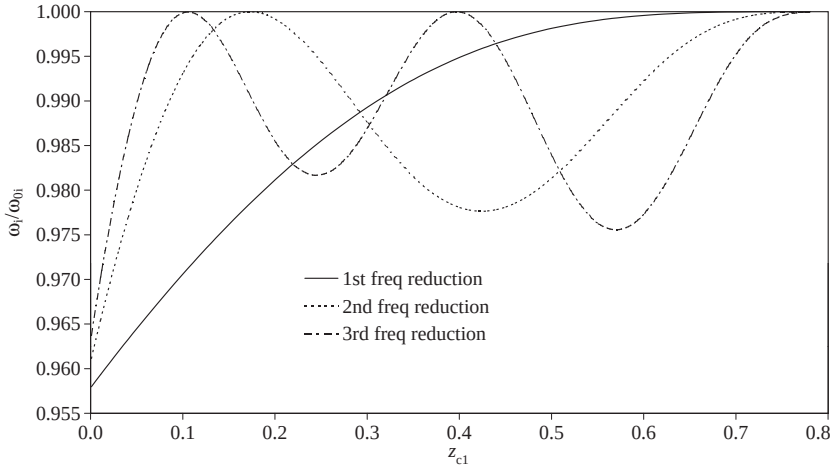

Fig. 15. Frequency reduction of a circular-hollow-sectional cantilever beam having an open crack at varying locations ($D_i/D_e = 0.5$).

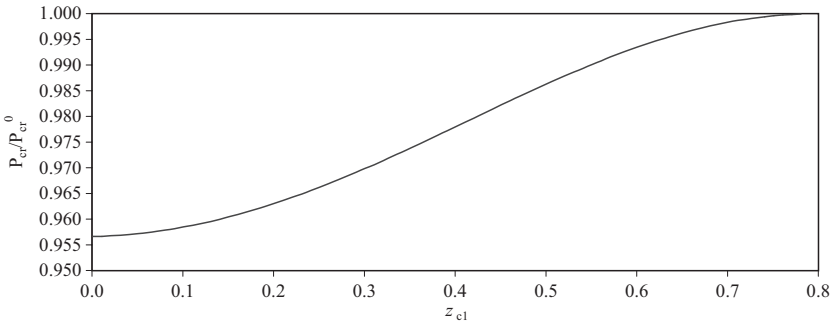

Fig. 16. Buckling-load reduction of a circular-hollow-sectional beam having an open crack at varying locations ($D_i/D_e = 0.5$).

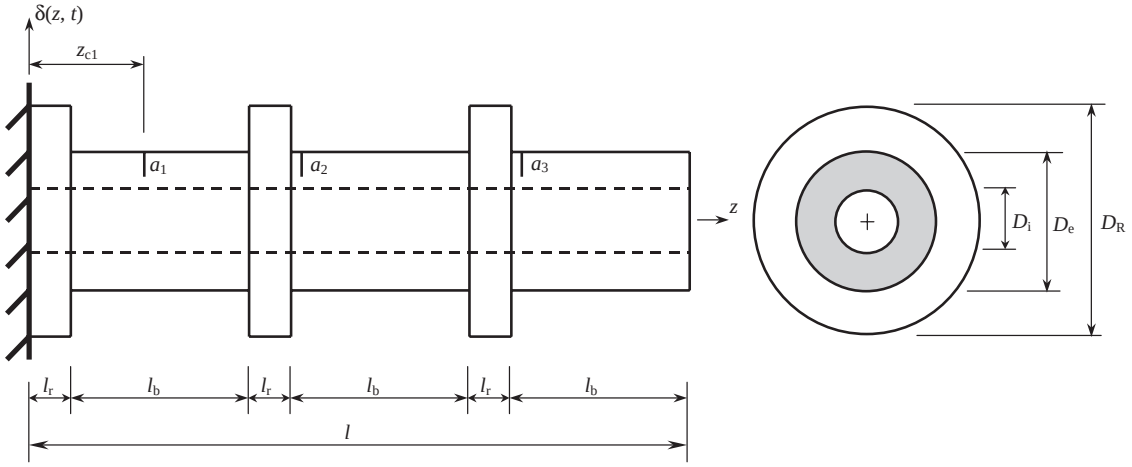

Fig. 17. A circular-hollow-sectional cantilever beam having three stiffening rings and three open cracks.

Fig. 16 stands for the buckling-load reduction, while the horizontal axis stands for the location of crack.

Example 5. *Vibration of a circular-hollow-sectional cantilever beam having stiffening rings and three open cracks.*

Fig. 17 shows a circular-hollow-sectional cantilever beam having three stiffening rings and three open cracks. The geometrical parameters for the beam are: $l = 0.66\,\text{m}$, $l_r = 0.02\,\text{m}$, $l_b = 0.2\,\text{m}$, $D_e = 0.03\,\text{m}$, $D_i = 0.0225\,\text{m}$, $D_R = 0.045\,\text{m}$. The material parameters are: $E = 210\,\text{GPa}$, $\mu = 0.33$, $\rho = 7800\,\text{kg/m}^3$. The three cracks have the same depth, i.e., $a_1 = a_2 = a_3 = 0.015\,\text{m}$. The second and third cracks are at different fixed locations, while the location of the first crack varies ($z_{c1} = 0.021\,\text{m} \sim 0.219\,\text{m}$). Results are shown in Fig. 18. The vertical axis in Fig. 18 stands for the natural frequency reduction, while the horizontal axis stands for the location of the first crack.

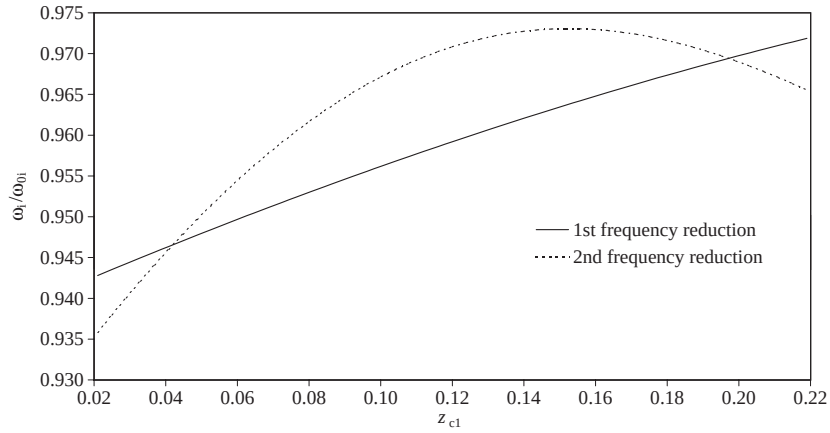

Fig. 18. Frequency reduction of a circular-hollow-sectional cantilever beam having three stiffening rings and three open cracks.

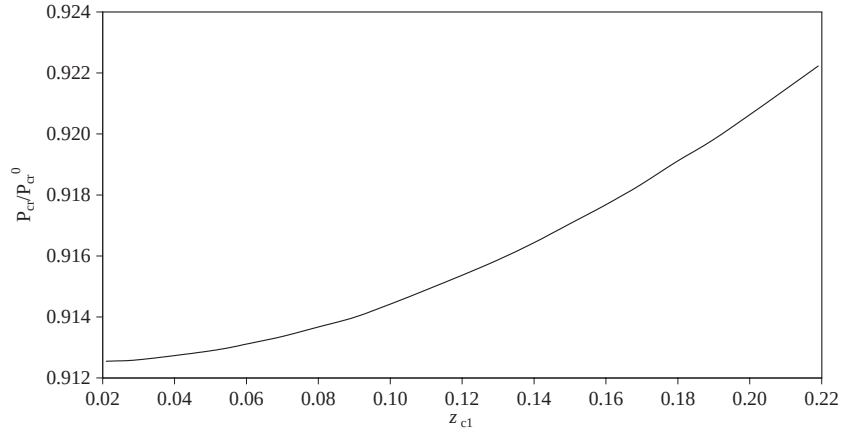

Fig. 19. Buckling-load reduction of a clamped beam with stiffening rings and three open cracks.

Example 6. *Stability of a circular-hollow-sectional cantilever beam having stiffening rings and three open cracks.*

The same beam as in Example 5 is considered. It has the same three cracks. The second and third cracks are at different fixed locations, while the location of the first crack varies ($z_{c1} = 0.021-0.219$ m). Results are shown in Fig. 19. The vertical axis in Fig. 19 stands for the buckling-load reduction, while the horizontal axis stands for the location of the first crack.

8. Conclusions and future work

Local flexibility coefficients due to the presence of an open sectional crack in rectangular- or circular-hollow-sectional beams are derived. The general formulae are in integral form. Explicit

formulae are obtained through Gauss quadrature and least-squares fitting. The best-fitted curves are also presented. The local flexibility coefficients are then employed for the vibration and stability analysis of cracked beams having rectangular or circular hollow sections under the assumption that the cracks are always open and the beam is in the range of linear elasticity. The usefulness and simplicity of the flexibility coefficients in the analysis are demonstrated in numerical examples. The authors will design and carry out some experiments to validate the analytical results obtained in this paper.

Appendix A. Best-fitted formulas for the local flexibility coefficients

Case 1. Solid rectangular cross-sectional beam:

$$\begin{aligned} CE'bh^2 \approx e^{1/(1-\zeta)}(&-0.2314\times10^{-4}\zeta + 52.3790\zeta^2 - 130.2463\zeta^3 \\ &+ 308.4111\zeta^4 - 602.1761\zeta^5 + 937.6805\zeta^6 \\ &- 1306.7397\zeta^7 + 1398.7523\zeta^8 - 1059.6215\zeta^9 \\ &+ 388.1628\zeta^{10}) \quad (\zeta = a/h, 0\leqslant\zeta\leqslant0.5,\ error<0.038\%). \end{aligned} \tag{A.1}$$

Case 2. Solid circular cross-sectional beam:

$$\begin{aligned} CE'D^3 \approx e^{1/(1-\zeta)}(&0.1687\times10^{-3}\zeta^{0.4} - 0.9770\times10^{-2}\zeta^{0.8} + 0.2382\zeta^{1.2} \\ &- 3.2016\zeta^{1.6} + 25.5385\zeta^2 - 58.1428\zeta^{2.4} \\ &+ 679.8828\zeta^{2.8} - 1350.4090\zeta^{3.2} + 794.0302\zeta^{3.6} \\ &- 11.3371\zeta^4) \quad (\zeta = a/D, 0\leqslant\zeta\leqslant0.1,\ error<0.045\%) \end{aligned} \tag{A.2a}$$

and

$$\begin{aligned} CE'D^3 \approx e^{1/(1-\zeta)}(&5.4931\zeta^{0.4} - 60.0706\zeta^{0.8} + 249.0679\zeta^{1.2} \\ &- 437.5001\zeta^{1.6} + 172.6435\zeta^2 - 55.5990\zeta^{2.4} \\ &+ 3036.1620\zeta^{2.8} - 7991.3829\zeta^{3.2} + 7992.1873\zeta^{3.6} \\ &- 2934.3483\zeta^4) \quad (\zeta = a/D, 0.1\leqslant\zeta\leqslant0.5,\ error<0.0064\%). \end{aligned} \tag{A.2b}$$

Case 3. Hollow circular cross-sectional beam:

$\gamma = D_i/D_e = 0.3,$

$$\begin{aligned} CE'D_e^3 \approx e^{1/(1-\zeta)}(&0.1588\times10^{-3}\zeta^{0.4} - 0.9274\times10^{-2}\zeta^{0.8} + 0.2279\zeta^{1.2} \\ &- 3.0843\zeta^{1.6} + 24.7144\zeta^2 - 53.2924\zeta^{2.4} \\ &+ 673.6523\zeta^{2.8} - 1340.2343\zeta^{3.2} + 773.0600\zeta^{3.6} \\ &+ 3.9297\zeta^4) \quad (\zeta = a/D_e,\ 0\leqslant\zeta\leqslant0.1,\ error<0.04\%), \end{aligned} \tag{A.3a}$$

$$CE'D_e^3 \approx e^{1/(1-\zeta)}(-1.5190\zeta^{0.4} + 48.0300\zeta^{0.8} - 505.7346\zeta^{1.2} + 2710.4929\zeta^{1.6} - 8489.3637\zeta^{2} + 16237.4386\zeta^{2.4} - 17821.2615\zeta^{2.8} + 9429.8274\zeta^{3.2} - 569.8074\zeta^{3.6} - 1058.8774\zeta^{4}) \quad (\zeta = a/D_e,\ 0.1 \leqslant \zeta \leqslant 0.35,\ error < 0.0009\%), \tag{A.3b}$$

$$CE'D_e^3 \approx e^{1/(1-\zeta)}(-7942.6668\zeta^{0.4} + 39626.3552\zeta^{0.8} - 65868.8104\zeta^{1.2} + 39605.9964\zeta^{1.6} - 14332.3830\zeta^{2} - 26166.7493\zeta^{2.4} + 199643.4402\zeta^{2.8} - 318149.0794\zeta^{3.2} + 187361.1532\zeta^{3.6} - 33346.8571\zeta^{4}) \quad (\zeta = a/D_e,\ 0.35 \leqslant \zeta \leqslant 0.5,\ error < 0.06\%) \tag{A.3c}$$

$\gamma = D_i/D_e = 0.5,$

$$CE'D_e^3 \approx e^{1/(1-\zeta)}(0.1790 \times 10^{-3}\zeta^{0.4} - 0.01045\zeta^{0.8} + 0.2567\zeta^{1.2} - 3.4736\zeta^{1.6} + 27.8300\zeta^{2} - 60.4683\zeta^{2.4} + 756.6548\zeta^{2.8} - 1505.2487\zeta^{3.2} + 870.8037\zeta^{3.6} + 1.8475\zeta^{4}) \quad (\zeta = a/D_e,\ 0 \leqslant \zeta \leqslant 0.1,\ error < 0.04\%), \tag{A.4a}$$

$$CE'D_e^3 \approx e^{1/(1-\zeta)}(-1.0060\zeta^{0.4} + 9.6107\zeta^{0.8} - 29.6192\zeta^{1.2} + 16.3389\zeta^{1.6} + 42.8801\zeta^{2} + 218.8186\zeta^{2.4} - 329.3538\zeta^{2.8} - 190.9792\zeta^{3.2} + 554.7871\zeta^{3.6} - 277.5391\zeta^{4}) \quad (\zeta = a/D_e,\ 0.1 \leqslant \zeta \leqslant 0.25,\ error < 0.0002\%), \tag{A.4b}$$

$$CE'D_e^3 \approx e^{1/(1-\zeta)}(-2429.5612\zeta^{0.4} + 10105.0170\zeta^{0.8} - 12608.8963\zeta^{1.2} + 23680.8521\zeta^{1.6} - 63973.7077\zeta^{2} - 29706.9774\zeta^{2.4} + 270762.9328\zeta^{2.8} - 169834.8546\zeta^{3.2} - 190849.3904\zeta^{3.6} + 171110.1644\zeta^{4}) \quad (\zeta = a/D_e,\ 0.25 \leqslant \zeta \leqslant 0.35,\ error < 0.09\%), \tag{A.4c}$$

$$CE'D_e^3 \approx e^{1/(1-\zeta)}(-96.9750\zeta^{0.4} + 448.3050\zeta^{0.8} - 615.4035\zeta^{1.2} + 33.1566\zeta^{1.6} + 644.3539\zeta^{2} - 612.6326\zeta^{2.4} + 1007.3750\zeta^{2.8} - 2437.5767\zeta^{3.2} + 2506.8430\zeta^{3.6} - 866.6797\zeta^{4}) \quad (\zeta = a/D_e,\ 0.35 \leqslant \zeta \leqslant 0.5,\ error < 0.09\%). \tag{A.4d}$$

$\gamma = D_i/D_e = 0.7,$

$$CE'D_e^3 \approx e^{1/(1-\zeta)}(0.2752 \times 10^{-3}\zeta^{0.4} - 0.01605\zeta^{0.8} + 0.3936\zeta^{1.2} - 5.3200\zeta^{1.6} + 42.5900\zeta^{2} - 93.0730\zeta^{2.4} + 1154.6563\zeta^{2.8} - 2296.4230\zeta^{3.2} + 1330.8476\zeta^{3.6} + 0.4202\zeta^{4}) \quad (\zeta = a/D_e,\ 0 \leqslant \zeta \leqslant 0.1,\ error < 0.04\%), \tag{A.5a}$$

$$CE'D_e^3 \approx e^{1/(1-\zeta)}(-444.4192\zeta^{0.4} - 527.5308\zeta^{0.8} + 34598.5310\zeta^{1.2} - 137888.5662\zeta^{1.6} - 31.0290\zeta^{2} + 851211.4274\zeta^{2.4} - 734003.7416\zeta^{2.8} - 3193126.772\zeta^{3.2} + 6889739.187\zeta^{3.6} - 3992249.482\zeta^{4}) \quad (\zeta = a/D_e,\ 0.1 \leqslant \zeta \leqslant 0.15,\ error < 0.007\%), \tag{A.5b}$$

$$CE'D_e^3 \approx e^{1/(1-\zeta)}(-2268.4084\zeta^{0.4} + 22777.3434\zeta^{0.8} - 98437.9691\zeta^{1.2} + 248059.5618\zeta^{1.6} - 439917.5520\zeta^{2} + 656597.2477\zeta^{2.4} - 855011.6438\zeta^{2.8} + 825060.9584\zeta^{3.2} - 474965.1588\zeta^{3.6} + 118270.8604\zeta^{4}) \quad (\zeta = a/D_e,\ 0.15 \leqslant \zeta \leqslant 0.35,\ error < 0.2\%). \tag{A.5c}$$

Case 4. Hollow rectangular cross-sectional beam:

$r_t = 0.35\ (r_b = 1.0)$,

$$CE'h_0^3 \approx e^{1/(1-\zeta)}(0.9903 \times 10^{-5}\zeta^{0.4} + 0.5643 \times 10^{-4}\zeta^{0.8} - 0.007191\zeta^{1.2} + 0.04106\zeta^{1.6} + 54.1775\zeta^{2} - 14.4993\zeta^{2.4} + 67.7718\zeta^{2.8} - 539.6241\zeta^{3.2} + 875.6370\zeta^{3.6} - 454.6942\zeta^{4}) \quad (\zeta = a/h_0,\ 0 \leqslant \zeta \leqslant 0.25,\ error < 0.0002\%), \tag{A.6a}$$

$$CE'h_0^3 \approx e^{1/(1-\zeta)}(3.0292\zeta^{0.4} - 16.5937\zeta^{0.8} + 22.5107\zeta^{1.2} + 12.4519\zeta^{1.6} + 47.5798\zeta^{2} - 78.6711\zeta^{2.4} - 52.7342\zeta^{2.8} - 17.2254\zeta^{3.2} + 364.3971\zeta^{3.6} - 298.8736\zeta^{4}) \quad (\zeta = a/h_0,\ 0.25 \leqslant \zeta \leqslant 0.35,\ error < 0.000007\%), \tag{A.6b}$$

$$CE'h_0^3 \approx e^{1/(1-\zeta)}(22.8246\zeta^{0.4} - 73.3424\zeta^{0.8} + 47.0626\zeta^{1.2} + 86.2010\zeta^{1.6} - 8.2983\zeta^{2} - 65.6099\zeta^{2.4} - 218.5020\zeta^{2.8} + 54.1675\zeta^{3.2} + 588.5319\zeta^{3.6} - 449.3343\zeta^{4}) \quad (\zeta = a/h_0,\ 0.35 \leqslant \zeta \leqslant 0.5,\ error < 0.00002\%). \tag{A.6c}$$

$r_t = 0.25\ \ (r_b = 1.0)$,

$$CE'h_0^3 \approx e^{1/(1-\zeta)}(0.8844 \times 10^{-4}\zeta^{0.4} - 0.004477\zeta^{0.8} + 0.09720\zeta^{1.2} - 1.2245\zeta^{1.6} + 69.6293\zeta^{2} - 55.4973\zeta^{2.4} + 183.4556\zeta^{2.8} - 784.0426\zeta^{3.2} + 1148.2809\zeta^{3.6} - 576.1615\zeta^{4}) \quad (\zeta = a/h_0,\ 0 \leqslant \zeta \leqslant 0.15,\ error < 0.002\%), \tag{A.7a}$$

$$CE'h_0^3 \approx e^{1/(1-\zeta)}(0.4835\zeta^{0.4} - 3.0114\zeta^{0.8} + 2.6941\zeta^{1.2} + 15.9130\zeta^{1.6} + 34.2396\zeta^{2} - 35.9424\zeta^{2.4} + 35.1120\zeta^{2.8} - 229.0307\zeta^{3.2} + 425.3254\zeta^{3.6} - 250.8735\zeta^{4}) \quad (\zeta = a/h_0,\ 0.15 \leqslant \zeta \leqslant 0.25,\ error < 0.00002\%), \tag{A.7b}$$

$$CE'h_0^3 \approx e^{1/(1-\zeta)}(-13.6117\zeta^{0.4} + 150.9723\zeta^{0.8} - 400.6208\zeta^{1.2} + 123.1813\zeta^{1.6} + 1013.5706\zeta^{2} - 1222.7133\zeta^{2.4} - 465.1126\zeta^{2.8} + 1387.3873\zeta^{3.2} - 411.1656\zeta^{3.6} - 175.1998\zeta^{4}) \quad (\zeta = a/h_0,\ 0.25 \leqslant \zeta \leqslant 0.5,\ error < 0.0003\%). \tag{A.7c}$$

$r_t = 0.15\ (r_b = 1.0)$,

$$CE'h_0^3 \approx e^{1/(1-\zeta)}(0.9269 \times 10^{-4}\zeta^{0.4} - 0.005320\zeta^{0.8} + 0.1305\zeta^{1.2} - 1.8137\zeta^{1.6} + 106.5995\zeta^{2} - 91.1370\zeta^{2.4} + 308.2441\zeta^{2.8} - 1260.5451\zeta^{3.2} + 1829.1508\zeta^{3.6} - 917.6437\zeta^{4}) \quad (\zeta = a/h_0,\ 0 \leqslant \zeta \leqslant 0.1,\ error < 0.001\%), \tag{A.8a}$$

$$CE'h_0^3 \approx e^{1/(1-\zeta)}(-302.2690\zeta^{0.4} - 360.1778\zeta^{0.8} + 23544.2601\zeta^{1.2} - 93809.7198\zeta^{1.6} - 4.3314\zeta^{2} + 579233.8955\zeta^{2.4} - 499877.7083\zeta^{2.8} - 2172413.395\zeta^{3.2} + 4688622.091\zeta^{3.6} - 2717071.081\zeta^{4}) \quad (\zeta = a/h_0,\ 0.1 \leqslant \zeta \leqslant 0.15,\ error < 0.005\%), \tag{A.8b}$$

$$CE'h_0^3 \approx e^{1/(1-\zeta)}(22.2136\zeta^{0.4} - 168.0020\zeta^{0.8} + 712.4735\zeta^{1.2} - 1948.6712\zeta^{1.6} + 3794.3229\zeta^{2} - 5694.8840\zeta^{2.4} + 7090.2229\zeta^{2.8} - 6962.5050\zeta^{3.2} + 4469.4318\zeta^{3.6} - 1327.0868\zeta^{4}) \quad (\zeta = a/h_0,\ 0.15 \leqslant \zeta \leqslant 0.5,\ error < 0.0003\%). \tag{A.8c}$$

References

[1] A.D. Dimarogonas, Vibration of cracked structures: a state of the art review, Engineering Fracture Mechanics 55 (1996) 831–857.
[2] T.G. Chondros, A.D. Dimarogonas, Identification of cracks in welded joints of complex structures, Journal of Sound and Vibration 69 (1980) 531–538.
[3] A.D. Dimarogonas, C.A. Papadopoulos, Vibration of cracked shafts in bending, Journal of Sound and Vibration 91 (4) (1983) 583–593.
[4] P. Gudmunson, The dynamic behaviour of slender structures with cross-sectional cracks, Journal of Mechanics and Physics of Solids 31 (1983) 329–345.
[5] S. Christides, A.D.S. Barr, One-dimensional theory of cracked Euler–Bernoulli beams, International Journal of Mechanical Science 26 (1984) 639–648.

[6] C.A. Papadopoulos, A.D. Dimarogonas, Coupled longitudinal and bending vibrations of a cracked shaft, Journal of Vibration, Acoustics, Stress, and Reliability in Design 110 (1988) 1–8.
[7] G. Gounaris, A.D. Dimarogonas, A finite element of a cracked prismatic beam for structural analysis, Computers and Structures 28 (1988) 309–313.
[8] B.S. Haristy, W.T. Springer, A general beam element for use in damage assessment of complex structures, Journal of Vibration, Acoustics, Stress and Reliability in Design 110 (1988) 389–394.
[9] P.F. Rizos, N. Aspragatos, A.D. Dimarogonas, Identification of crack location and magnitude in a cantilever beam from the vibration modes, Journal of Sound and Vibration 138 (1990) 381–388.
[10] G.L. Qian, S.N. Gu, J.S. Jiang, The dynamic behaviour and crack detection of a beam with a crack, Journal of Sound and Vibration 138 (1990) 233–243.
[11] W.M. Ostachowicz, M. Krawczuk, Analysis of the effect of cracks on the natural frequencies of a cantilever beam, Journal of Sound and Vibration 150 (1991) 191–201.
[12] R.Y. Liang, J. Hu, F. Choy, Theoretical study of crack-induced eigenfrequency changes on beam structures, Journal of Engineering Mechanics 118 (1992) 384–396.
[13] R.Y. Liang, J. Hu, F. Choy, Quantitative NDE techniques for assessing damages in beam structures, Journal of Engineering Mechanics 118 (1992) 1468–1487.
[14] R.Y. Liang, F. Choy, J. Hu, Detection of cracks in beam structures using measurements of natural frequencies, Journal of the Franklin Institute 328 (1991) 505–518.
[15] J. Hu, R.Y. Liang, An integrated approach to detection of cracks using vibration characteristics, Journal of the Franklin Institute 330 (1993) 841–853.
[16] Y. Narkis, Identification of cracks' location in vibrating simply supported beams, Journal of Sound and Vibration 172 (1993) 549–558.
[17] A. Morassi, Crack-induced changes in eigenfrequencies of beam structures, Journal of Engineering Mechanics 119 (1993) 1768–1803.
[18] E.I. Shifrin, R. Ruotolo, Natural frequencies of a beam with an arbitrary number of cracks, Journal of Sound and Vibration 222 (1999) 409–423.
[19] T.Y. Kam, T.Y. Lee, Detection of cracks in structures using modal test data, Engineering Fracture Mechanics 42 (1992) 381–387.
[20] D.Y. Zheng, S.C. Fan, Natural frequencies of a non-uniform beam with multiple cracks via modified Fourier series, Journal of Sound and Vibration 242 (4) (2001) 701–717.
[21] D.Y. Zheng, S.C. Fan, Natural frequency changes of a cracked Timoshenko beam by modified Fourier series, Journal of Sound and Vibration 246 (2) (2001) 297–317.
[22] S.C. Fan, D.Y. Zheng, F.T.K. Au, Gibbs phenomenon free Fourier series for vibration and stability of complex beams, American Institute of Aeronautics and Astronautics Journal 39 (10) (2001) 1977–1984.
[23] J. Kong, W.L. Cleghorn, Free vibration of cracked plates using finite strip method, The Eighth East Asia-Pacific Conference on Structural Engineering and Construction, December 5–7, Singapore, 2001.
[24] Z.H. Liu, G.X. Dong, W.A. Wang, Fundamentals of Anti-Fracture Design of Engineering Structures, Huazhong University of Science and Technology Press, Wuhan, P.R. China, 1990 (in Chinese).
[25] H. Tada, P.C. Paris, G.R. Irwin, The Stress Analysis of Cracks Handbook, ASME Press, New York, USA, 2000.
[26] G. Evans, Practical Numerical Integration, Wiley, New York, 1993.
[27] M.L. James, G.M. Smith, J.C. Wolford, Applied Numerical Methods for Digital Computation, Harper Collins College Publishers, New York, 1993.
[28] J.Y. Liu, D.Y. Zheng, Z.J. Mei, Practical Integral Transforms in Engineering, Huazhong University of Science and Technology Press, Wuhan, P.R. China, 1995 (in Chinese).
[29] D.Y. Zheng, Y.K. Cheung, F.T.K. Au, Y.S. Cheng, Vibration of multi-span non-uniform beams under moving loads by using modified beam vibration functions, Journal of Sound and Vibration 212 (1998) 455–467.
[30] F.T.K. Au, D.Y. Zheng, Y.K. Cheung, Vibation and stability of non-uniform beams with abrupt changes of cross-section by using C^1 modified beam vibration functions, Applied Mathematical Modeling 29 (1999) 19–34.
[31] Y.K. Cheung, F.T.K. Au, D.Y. Zheng, Analysis of deep beams and shear walls by finite strip method with C^0 continuous displacement functions, Thin Walled Structures 32 (1998) 289–303.

[32] Y.K. Cheung, F.T.K. Au, D.Y. Zheng, Y.S. Cheng, Vibration of multi-span non-uniform bridges under moving vehicles and trains by using modified beam vibration functions, Journal of Sound and Vibration 228 (1999) 611–628.
[33] D.Y. Zheng, Vibration and Stability Analysis of Plate-Type structures under Moving Loads by Analytical and Numerical Methods, Ph.D. Thesis, The University of Hong Kong, 1999.
[34] Y.K. Cheung, F.T.K. Au, D.Y. Zheng, Finite strip method for the free vibration and buckling analysis of plates with abrupt changes in thickness and complex support conditions, Thin-Walled Structures 36 (2000) 89–110.